Approaching the Hole Mobility Limit of GaSb Nanowires

Zai-xing Yang,[†,‡,§] SenPo Yip,[†,‡,§] Dapan Li,[†,§] Ning Han,[*,‖] Guofa Dong,[†,§] Xiaoguang Liang,[†,§] Lei Shu,[†] Tak Fu Hung,[†] Xiaoliang Mo,[⊥] and Johnny C. Ho[*,†,‡,§]

[†]Department of Physics and Materials Science, City University of Hong Kong, 83 Tat Chee Avenue, Kowloon 999077, Hong Kong, [‡]State Key Laboratory of Millimeter Waves, City University of Hong Kong, 83 Tat Chee Avenue, Kowloon 999077, Hong Kong, [§]Shenzhen Research Institute, City University of Hong Kong, Shenzhen 518057, P. R. China, [‖]State Key Laboratory of Multiphase Complex Systems, Institute of Process Engineering, Chinese Academy of Sciences, Beijing 100190, P. R. China, and [⊥]Department of Materials Science, 220 Handan Road, Fudan University, Shanghai 200433, P. R. China

ABSTRACT In recent years, high-mobility GaSb nanowires have received tremendous attention for high-performance p-type transistors; however, due to the difficulty in achieving thin and uniform nanowires (NWs), there is limited report until now addressing their diameter-dependent properties and their hole mobility limit in this important one-dimensional material system, where all these are essential information for the deployment of GaSb NWs in various applications. Here, by employing the newly developed surfactant-assisted chemical vapor deposition, high-quality and uniform GaSb NWs with controllable diameters, spanning from 16 to 70 nm, are successfully prepared, enabling the direct assessment of their growth orientation and hole mobility as a function of diameter while elucidating the role of sulfur surfactant and the interplay between surface and interface energies of NWs on their electrical properties. The sulfur passivation is found to efficiently stabilize the high-energy NW sidewalls of (111) and (311) in order to yield the thin NWs (*i.e.*, <40 nm in diameters) with the dominant growth orientations of ⟨211⟩ and ⟨110⟩, whereas the thick NWs (*i.e.*, >40 nm in diameters) would grow along the most energy-favorable close-packed planes with the orientation of ⟨111⟩, supported by the approximate atomic models. Importantly, through the reliable control of sulfur passivation, growth orientation and surface roughness, GaSb NWs with the peak hole mobility of $\sim$400 $cm^2 V^{-1} s^{-1}$ for the diameter of 48 nm, approaching the theoretical limit under the hole concentration of $\sim 2.2 \times 10^{18}$ cm^{-3}, can be achieved for the first time. All these indicate their promising potency for utilizations in different technological domains.

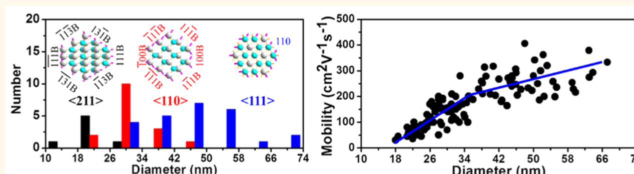

KEYWORDS: GaSb nanowires · surfactant-assisted chemical vapor deposition · diameter dependent · growth orientation · hole mobility

In the past decades, because of the unique physical properties, III–V semiconductor nanowires (NWs) have attracted extensive research interests and are recognized as promising fundamental building blocks for next-generation electronics, photonics, photovoltaics and so on.[1−15] In particular, as a technologically important p-type semiconductor, increasingly more attention has been focused on GaSb NWs owing to their intermediate band gap ($\sim$0.726 eV) and the highest hole mobility ($\mu_h \sim 1000$ $cm^2 V^{-1} s^{-1}$) among all III–V materials.[10,16−22] For instance, the InGaSb NWs fabricated *via* complicated "top-down" techniques from single-crystalline InGaSb wafers have been demonstrated with the excellent hole mobility up to 370 $cm^2 V^{-1} s^{-1}$;[20] however, the typical GaSb NWs grown by "bottom-up" methods (*e.g.*, chemical vapor deposition, CVD) *via* the vapor–liquid–solid (VLS) and vapor solid–solid (VSS) growth mechanisms give relatively low mobility (<30 $cm^2 V^{-1} s^{-1}$), which can be attributed to the poor crystal quality as well as the nonstoichiometry induced by the uncontrollable radial NW growth.[22−26] This uneven lateral overgrowth is often yielded by the surface accumulation of Sb precursors coming from the Gibbs–Thomson effect such that tapered and thick NWs are easily obtained in the different vapor–solid (VS) growth mechanism.[22,25−30] Even when the thin InAs NW stems are employed as the growing template, much thicker GaSb NWs are epitaxially attained. It is therefore challenging to achieve crystalline GaSb NWs with controlled diameter and length.

Regardless, it is critical to have a good control of these NW dimensions since the growth orientation and their corresponding physical properties are found highly dependent on their diameters. Si and ZnSe NWs

* Address correspondence to johnnyho@cityu.edu.hk, nhan@ipe.ac.cn.

Received for review July 7, 2015 and accepted August 16, 2015.

Published online August 17, 2015
10.1021/acsnano.5b04152

© 2015 American Chemical Society

are observed to display the size-dependent growth direction from ⟨111⟩ to ⟨110⟩ for the decreasing diameter, which can be interpreted based on the interplay between the surface and interface energies of the NWs,[31−33] whereas the trend is opposite for the case of GaAs NWs due to the varied Ga diffusion in different Ga supersaturation in the catalytic alloy tips during the NW growth.[34,35] At the same time, the carrier mobility of InAs, GaN and InGaAs NWs would also get degraded monotonically as the diameter is reduced, caused by the serious surface scattering in the miniaturized NWs with the higher surface-to-volume ratio.[36−38] In any case, owing to the difficulty in realizing the thin and high-performance GaSb NWs down to a few tens of nanometers, there is only limited report until now addressing their diameter-dependent growth orientation and physical properties, especially the hole mobility limit in this one-dimensional material system, in which all these are essential information for the practical utilization of GaSb NWs in various applications.

In our previous work, we have developed the use of sulfur surfactant in CVD to accomplish very thin and uniform GaSb NWs on amorphous substrates with the diameters below 20 nm.[21] The sulfur atoms are contributed to form stable S−Sb bonds on the as-grown NW surface in passivating the sidewalls and alleviating the uncontrolled lateral NW growth. However, it is still not explicitly clear about the passivating effect of these surfactant on different NW surface crystal planes, NW growth orientation, and their hole mobilities. Importantly, this surfactant-assisted technique can also allow us to obtain high-quality GaSb NWs with the tailorable dimension to evaluate their size-dependent properties and performance limits. Here, we adopt and extend the past work to attain crystalline GaSb NWs with varied diameters ranging from 16 to 70 nm, therefore, enabling the direct assessment of their growth orientation and hole mobility as a function of the diameter while elucidating the role of sulfur surfactant and the interplay between the surface and interface energies of NWs on their electrical properties. By exploiting the appropriate surface passivation, when configured into the field-effect transistor (FET), we find that the GaSb NW exhibits a record high peak hole mobility of $\sim$400 cm^2 V^{-1} s^{-1} for the diameter of 48 nm, approaching the theoretical mobility limit under the hole concentration of $\sim$2.2 $\times$ 10^{18} cm^{-3}.[39,40] All these results would not only affirm the effectiveness of our surfactant-assisted CVD technique but also provide a valuable insight in achieving high-performance GaSb NWs for technological applications.

RESULTS AND DISCUSSION

One typical method to effectively control the diameter of as-grown NWs is to utilize metal catalytic films with different thicknesses during the CVD growth.[34,35,41]

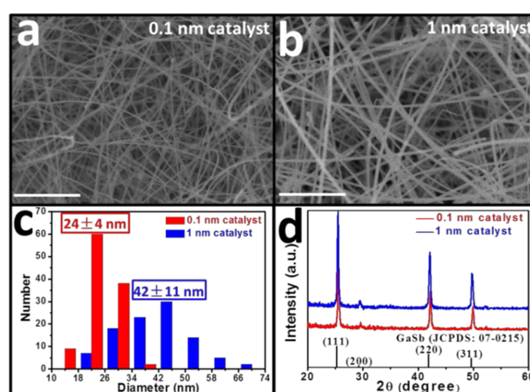

Figure 1. Morphology, diameter distribution, and crystal structure of the as-prepared GaSb NWs. (a and b) SEM images of GaSb NWs prepared by using the 0.1 and 1 nm thick Au films as the catalyst (all scale bars are 1 μm). (c) Diameter distribution histogram and (d) XRD patterns of the grown NWs.

In this work, employing the recently developed sulfur-assisted solid-source CVD, we used Au films of 0.1 and 1 nm in thickness as the catalyst to achieve the growth of GaSb NWs with different diameter distributions. We note that the process condition, such as the amount of sulfur hired, carrier gas flow rate, source, and substrate temperatures, is maintained the same in all these growth runs in order to yield a consistent comparison for the subsequent studies. As shown in the SEM images (Figure 1a,b), it is obvious that both types of as-prepared GaSb NWs are straight, smooth, and dense with the length larger than 10 μm with varied diameters. On the basis of the diameter statistics of more than 100 NWs (Figure 1c), the thin NWs with a narrow diameter distribution of 24 $\pm$ 4 nm can be prepared by using the 0.1 nm thick Au catalytic film (red curve). While using a thicker catalytic film of 1 nm (blue curve), the as-prepared NWs become larger in the diameter along with a wider distribution (42 $\pm$ 11 nm), which is attributable to the bigger and more broadly dispersed Au catalytic seeds formed at the beginning of the NW growth. This phenomenon was also commonly observed in the CVD synthesis of other III−V NWs, including GaAs and InAs NWs.[42,43] In any case, it is clearly confirmed that the sulfur surfactant exploited here can effectively prohibit the uncontrolled radial growth of GaSb NWs, and thus, the obtained NWs are far thinner than those grown without the surfactant.[22,25,26] Furthermore, the phase purity and crystal structures of the grown NWs are also studied by XRD and all of them consist of the pure zinc-blende crystal structure, having $a = b = c = 0.6095$ nm (JCPDS Card No. 07-0215) (Figure 1d). This high phase purity indicates that there is no other impurity phases present such as those of the hexagonal wurtzite phase of GaSb or phases of Sb_xO_y and Ga_xO_y. At the same time, to further assess the crystallinity and chemical stoichiometry of the as-grown NWs, high-resolution transmission electron microscopy (HRTEM) and energy-dispersive

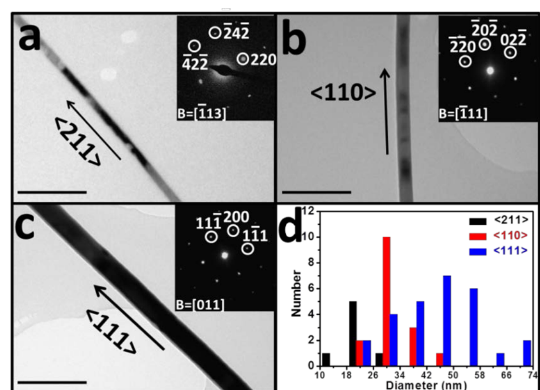

Figure 2. Diameter-dependent growth orientations of the as-prepared GaSb NWs. (a−c) TEM and SAED (inset) images of the NWs with growth directions of ⟨211⟩, ⟨110⟩, and ⟨111⟩, respectively (all scale bars are 200 nm). (d) Statistics of the NW growth direction as a function of the NW diameter.

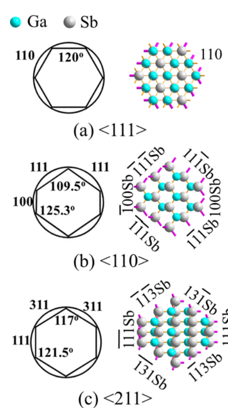

Figure 3. Schematics and approximate atomic models of the cross-section of zinc-blende GaSb NWs with different growth directions. (a) NWs grown in ⟨111⟩ directions have the surface composed of six crystal planes of (110), (b) NWs grown in ⟨110⟩ directions consisted of four crystal planes of (111) and two crystal planes of (100), and (c) NWs grown in ⟨211⟩ directions consisted of four crystal planes of (311) and two crystal planes of (111).

X-ray spectroscopy (EDS) are performed as illustrated in Supporting Information Figure S1. In accordance with our previous results,[21] the attained NWs are highly crystalline following a classical vapor−liquid−solid (VLS) or vapor−solid−solid (VSS) growth mode with a balanced stoichiometry (Ga/Sb ~ 1:1) in the NW body. More importantly, this controllable wide diameter range of high-quality GaSb NWs, spanning from 16 to 70 nm, would facilitate the direct evaluation of diameter-dependent properties of GaSb NWs successively performed.

To shed light in investigating the growth orientations of these NWs, selected area electron diffraction (SAED) in combination with TEM were utilized to characterize the NW growth direction as depicted in Figure 2. Figure 2a−c gives the typical TEM images of individual GaSb NWs with the diameter of 18, 38, and 67 nm with the growth directions of ⟨211⟩, ⟨110⟩, and ⟨111⟩, respectively. Figure 2d displays the statistics of growth direction of more than 50 NWs and it is evidently noticed the growth orientation of ⟨211⟩ is highly preferred when the NW diameter is smaller than 20 nm. For the intermediate diameter between 20 and 40 nm, NWs grow mainly along the ⟨110⟩ direction, while for the thick NWs above 40 nm in the diameter, the ⟨111⟩ direction would become dominant. All these findings are in a distinct contrast to the diameter-dependent growth orientation of Si and ZnSe NWs, in which the growth direction of <110>, < 211> and <111> are dominant for the small, medium and thick NWs there,[31−33] attributable to the interplay between the surface and interface energies of the NWs. They are also different to the case of GaAs NWs, where ⟨111⟩ orientations are favored for the thin NWs and ⟨110⟩ directions are preferred for the thick NWs, due to the altered Ga diffusion in different supersaturated Au−Ga alloy seeds with different dimensions.[34] In this case of GaSb NWs, since the Ga supersaturation observed in the catalytic tip is similar to the ones in GaAs NWs (Figure S1), the sulfur surfactant employed here to stabilize the NW sidewall during the CVD growth may somehow modify the surface energy of NW crystal planes, affecting the interplay between the surface and interface energies of the NWs and yielding this unique size-dependent growth orientation relation, with further examination required.

In this regard, a semiquantitative model is proposed in this work in order to evaluate the effect of sulfur surfactant on the surface energy of GaSb NWs with different growth orientations and surface crystal planes. Figure 3 gives the detailed schematics and approximate atomic models of the cross-section of NWs with various growth directions and their corresponding exposed surface planes. On the basis of our previous findings, the sulfur surfactant mainly forms covalent bonds of Sb−S for the NW surface passivation, while the surface Ga atoms are often oxidized forming Ga−O bonds.[21] This way, we would only take into account the possible configuration of dangling bonds (DBs) associated with surface Sb atoms on each crystal plane, which are preferable for the sulfur passivation. As shown in Figure 3, considering the zinc-blende crystal structure here, there are six equivalent nonpolar surface planes of (110) along the ⟨111⟩ oriented NWs, all separated by an angle of 120° and with only one Sb DB connected to each surface Sb atom (also see details in Supporting Information Figure S2b), contributing to the lowest density of DBs among all surface planes. This lowest DB density (*i.e.*, the lowest surface energy) would typically make the NW grown in ⟨111⟩ directions as reported by others.[22,23,44] Similarly, all the DB density can be calculated for each plane and compiled in Table 1 (see details in Supporting Information Figures S2 and S3). It is noted that the ⟨110⟩ and ⟨211⟩ oriented NWs would all have polar surface planes with the Sb termination due to the high V/III ratio required

TABLE 1. Summary of Sb Dangling Bonds (DBs) Existed on the NW Surfaces with Different Growth Orientations

NW growth orientation	NW surface planes	DB density (/nm^2)	required sulfur coordination number
111	(110) × 6	1/0.26 = 3.8	1
110	(111)Sb × 2	1/0.16= 6.2	1
	−(111)Sb × 2	3/0.16 = 18.6	3
	(100)Sb x 2	2/0.19 = 10.5	2
211	(111)Sb × 1	1/0.16 = 6.2	1
	−(111)Sb × 1	3/0.16 = 18.6	3
	(311)Sb × 2	2/0.31= 6.4	2
	−(311)Sb × 2	3/0.31 = 9.6	2

for the CVD growth.[27,28] In particular, there are four surface planes of (111)Sb and two surface planes of (100)Sb along the ⟨110⟩ oriented NWs, and four surface planes of (311)Sb and two surface planes of (111)Sb along the ⟨211⟩ oriented NWs, yielding the relatively higher DB density there. These higher surface energies would result in the NWs that are hardly grown in the direction of ⟨110⟩ and ⟨211⟩. However, when passivated by the sulfur surfactant, these Sb-terminated polar surface planes with the high DB density would become thermodynamically stable and especially favorable for the growth of thin NWs owing to the large surface-to-volume ratio. Because of the required valence coordination, the surface passivation with sulfur on the ⟨211⟩ oriented NWs would be more effective as compared to the ⟨110⟩ oriented counterparts (Supporting Information Figure S2). In any case, all these illustrate that the sulfur passivation can efficiently modulate the interplay between the surface and interface energies of the GaSb NWs by stabilizing the high-energy surface planes of (111), (311) and such to give the surface-stabilized thin NWs with the dominant growth orientation of ⟨211⟩ as well as the medium-sized NWs grown in the direction of ⟨110⟩ (*i.e.*, "surface effect" dominated). As the surface effect is not that prominent for the thick NWs, they would still be grown along the most energy-favorable close-packed planes with the orientation of ⟨111⟩ (*i.e.*, "bulk effect" dominated).

To validate this proposed model, X-ray photoelectron spectroscopy (XPS) is employed to study the surface bonding environment of the GaSb NWs. All the XPS spectra of the as-prepared NWs are calibrated with the reference peak of C 1s (285 eV). The relatively small shifting of the spectra can be attributed to the size effect as reported in the literatures,[45,46] which is not emphasized herein. As shown in Figure 4, the red and blue curves give the spectra of S 2s, Ga 3d, and Sb 4d of the thin and thick GaSb NWs prepared by using the 0.1 and 1 nm thick Au film as the catalyst, respectively. It is obvious that the S atoms are bounded on the surface of both thin and thick NWs in accordance with our previous study (Figure 4a).[21] The Gauss−Lorentz fitted spectra of Ga 3d and Sb 4d can also be found

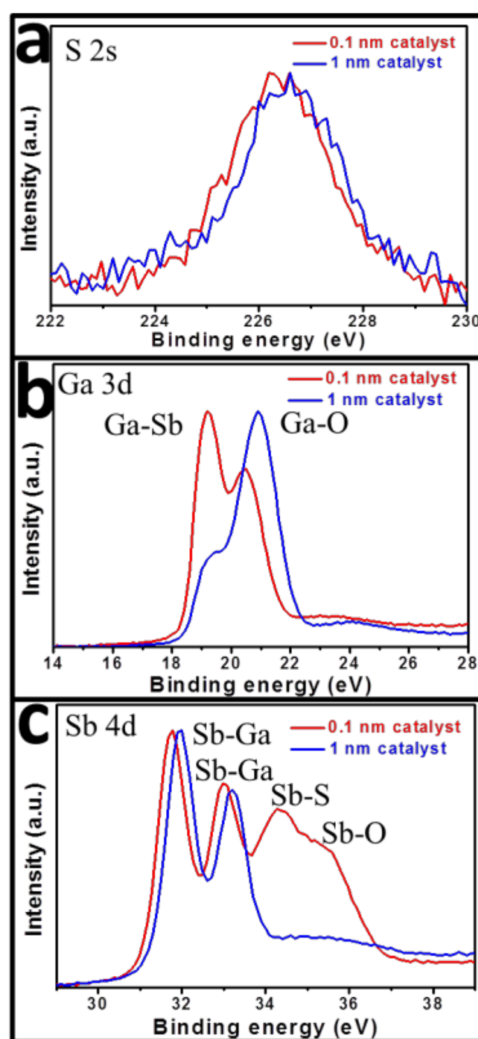

Figure 4. Surface elemental analysis of the as-prepared GaSb NWs. Red curves designate the S 2s, Ga 3d, and Sb 4d bonding regions of NWs prepared by using the 0.1 nm thick Au film as the catalyst, while the blue curves signify the S 2s, Ga 3d, and Sb 4d bonding regions of NWs prepared by using the 1 nm thick Au film as the catalyst. (a−c) XPS spectra of S 2s, Ga 3d, and Sb 4d of the NWs, respectively.

in Supporting Information Figure S4. Interestingly, the chemical binding nature of the surface Ga and Sb atoms are distinguishingly different between these two types of GaSb NWs (Figure 4b,c). The thin NWs possess the surface Ga atoms forming covalent bonds of Ga−Sb more dominantly than the ones of Ga−O, while the residual surface Sb atoms as well contribute a significant amount of the Sb−S and Sb−O bonds. In contrast, the thick NWs are observed to have more surface Ga−O bonds and an insignificant amount of the Sb−S and Sb−O bonds is resolved. All these indicate that the Sb−S bonds are more stable and noticeable on the thin GaSb NWs in passivating the exposed surfaces as compared to the ones of thick NWs, supporting the above proposed model in achieving the thin GaSb NWs *via* the surface stabilization with sulfur surfactant during the CVD growth while

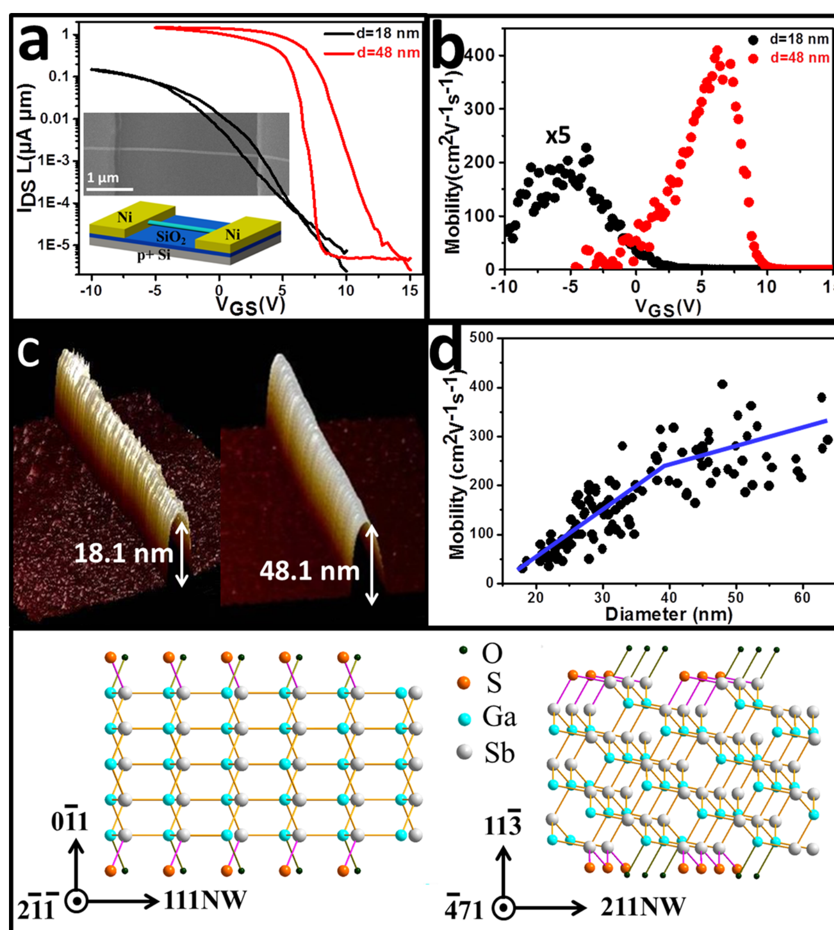

Figure 5. Electrical characterization of GaSb NWFETs with different NW dimensions. (a) Log scale $I_{DS}-V_{GS}$ characteristics of two representative back-gated GaSb NWFETs with NW diameters of 18 and 48 nm, respectively (V_{DS} = 0.1 V). The insets give the corresponding SEM image of the device as well as the device schematic with Ni metal contacts. (b) Field-effect hole mobility assessment for the same set of NWFETs presented in the panel (a) with V_{DS} = 0.1 V. (c) Three-dimensional AFM topography images for the diameter determination of NWs (*i.e.*, 18 and 48 nm in the diameter). (d) Peak field-effect hole mobility as a function of NW diameter, with the diameters ranging from 18 to 65 nm. (e) An atomic model illustrating the exposed sidewalls of ⟨111⟩ and ⟨211⟩ orientated NWs, where the intrinsically rough (311) surface is clearly shown for the thin ⟨211⟩ NWs, in a distinct contrast to the naturally smooth (110) surface of the thicker ⟨111⟩ NWs.

attaining the thick NWs grown along the close-packed direction.

Apart from affecting the NW growth orientation, the sulfur passivation is also expected to significantly influence the electrical properties of NWs with different diameters and growth directions. Here, global back-gate NWFETs with different NW dimensions are fabricated and thoroughly characterized. Long channel devices with the length >1 μm are utilized to ensure that the diffusive transport of carriers, rather than the ballistic or quasi-ballistic transport, are assessed, in which the intrinsic transport properties such as the carrier mobility can be deduced. As depicted in the transfer characteristics of two representative NWFET devices with the NW diameters of 18 and 48 nm (Figure 5a), the typical p-type conduction is exhibited and the ON current density is observed to be higher for the thick NWs along with a high ON/OFF current ratio up to 10^5. At the same time, the output characteristics of these NW devices are also given in Supporting Information Figure S5, confirming the ohmic contact formation with Ni source/drain electrodes. Meanwhile, the corresponding field-effect mobility can be calculated by a well-accepted method based on the square law model.[36] When we use the low-bias (*i.e.*, V_{DS} = 0.1 V) transconductance extracted from the transfer characteristics, $g_m = (dI_{DS})/(dV_{GS})|V_{DS}$, and the analytical expression, $\mu = g_m(L^2/C_{OX})(1/V_{DS})$, where C_{OX} is the gate capacitance obtained from the finite element analysis software COMSOL with respect to different NW diameters,[22,36] the field-effect mobility of individual NWs can be obtained reliably once the NW channel length and diameter are known (see details in Supporting Information). As shown in Figure 5b,c, the peak hole mobility of the thin NW (*i.e.*, 18 nm in the diameter) is found only ~40 $cm^2\ V^{-1}\ s^{-1}$, while it is promoted to ~400 $cm^2\ V^{-1}\ s^{-1}$ for the thick NW (*i.e.*, 48 nm in the diameter), approaching the theoretical mobility limit of GaSb under the estimated hole concentration of $n_h \sim 2.2 \times 10^{18}\ cm^{-3}$.[39,40] The hole concentration can be assessed by the equation,

TABLE 2. Comparison of Mobility and Other Physical Properties of Different p-type Sb-Based Nanowire FETs

materials	growth method	diameter (nm)	surface morphology	peak mobility ($cm^2/(V\ s)$)	concentration (cm^{-3})	reference
GaSb	Metalorganic CVD	91	Tapering			23
GaSb	CVD	130		14.2	2.2×10^{18}	25
GaSb	CVD	179	Tapering	30	9.7×10^{17}	22
Carbon-doped InSb	CVD	55	No tapering	140	$\sim 7.5 \times 10^{17}$	3
GaSb	Surfactant-assisted CVD	32	No tapering	∼200	3.1×10^{18}	21
GaSb	*Surfactant-assisted CVD*	*48*	*No tapering*	*∼400*	2.2×10^{18}	*This work*

$n_h = Q/(q\pi r^2 L) = (C_{OX}V_{th})/(q\pi r^2 L)$, where r is the NW radius and V_{th} is the threshold voltage. It is worth pointing out that this hole mobility value produces another record for the bottom-up prepared GaSb NWs in the literature (Table 2), and is even higher than those of top-down etched InGaSb NWs fabricated from the single-crystalline wafers.[20] Notably, the similar high mobility values are also found for several other NWs in the diameter range of 40−65 nm as demonstrated in the hole mobility statistics (Figure 5d). Although there is a small wire-to-wire variety, the function of hole mobility *versus* NW diameter (d spanning from 18 to 65 nm) clearly indicates an increase of mobility as the NWs grow thicker; however, it is interesting to find that there is an inflection point at the NW diameter of around 40 nm. That is, NWs with the diameter smaller than 40 nm would have their increasing trend of mobility more profound than the ones with diameter larger than 40 nm. Surprisingly, all these observations match well with the size-dependent growth orientation of GaSb NWs discussed above, which suggests that this mobility inflection may be correlated to the changes of NW orientation between the bulk-effect dominated ⟨111⟩ direction and the surface-effect dominated ⟨211⟩ direction. In other words, the surface-stabilized thin NWs grown in the ⟨211⟩ orientation (*i.e.*, with NW diameters <40 nm) would have the mobility more sensitive to the change in diameter as compared to their thick counterparts, and this larger sensitivity in these thin NWs is believed to be due to the enhanced surface scattering effect in the miniaturized NW geometry with the larger surface-to-volume ratio.[36,37] It is also noted that the surface roughness is another important factor disturbing the carrier mobility of NWs.[47] As demonstrated in Figure 5e, the thin GaSb NWs predominantly grown in the ⟨211⟩ direction would have the intrinsically rougher surface planes exposed as compared to the ones of thicker ⟨111⟩ oriented NWs, which is perfectly consistent to the experimental results obtained for the NW roughness determination in Figure 5c. One could expect that the mobility of thin NWs can be further enhanced here by controlling their growth orientations with less surface roughness. Anyway, utilizing the surfactant-assisted CVD in this diameter-dependent growth orientation and mobility study of GaSb NWs, a further insight among the effect of growth orientation, surface passivation and roughness on the NW carrier mobility can be readily obtained. By controlling all these important factors discussed above, the high-performance GaSb NW with the peak hole mobility of ∼400 $cm^2\ V^{-1}\ s^{-1}$, approaching the theoretical limit for the diameter of 48 nm, can be achieved for the first time, which highly illustrate their promising potency for different technological applications.

CONCLUSIONS

In conclusion, when we employ the different thickness of Au catalyst films, high-quality and uniform GaSb NWs with controllable diameters spanning from 16 to 70 nm can be successfully prepared by the surfactant-assisted CVD. The sulfur surfactant is found to play an important role in regulating the NW growth orientation due to the altered surface passivation effect on different exposed NW surface crystal planes with varied dangling bond density and atomic configuration. All these modified interplay between the surface and interface energies would yield the thin NWs (*i.e.*, ∼20 nm in diameters) preferentially grown along the ⟨211⟩ direction, medium sized NWs (*i.e.*, diameters between 20 and 40 nm) adopted in the ⟨110⟩ orientation and thick NWs (*i.e.*, >40 nm in diameters) taken along the ⟨111⟩ direction. Importantly, through the effective surface passivation by sulfur as well as controlling the NW growth orientation and surface roughness, GaSb NWs with the peak hole mobility up to 400 $cm^2\ V^{-1}\ s^{-1}$, approaching the theoretical limit under the estimated hole concentration of $\sim 2.2 \times 10^{18}\ cm^{-3}$, can be readily achieved. All these have demonstrated their promising prospect for next-generation high-mobility nanoelectronics.

MATERIALS AND METHODS

Nanowire Synthesis. GaSb NWs studied here are grown by employing a sulfur surfactant-assisted solid-source CVD method reported in our previous work.[21] In short, the solid powders of GaSb (99.999% purity) and sulfur (99.99% purity) are used as the source materials. A dual-zone horizontal tube furnace, one zone for the solid source (upstream) and one zone for the growth substrate (downstream), is used as the reactor for the synthesis

of GaSb NWs. Specifically, Au films with 0.1 and 1 nm thickness are utilized as catalysts for GaSb NW growth. At first, the Au thin films are predeposited on Si/SiO_2 substrates (50 nm thick thermally grown) and then the substrates are placed in the middle of the downstream zone. The solid sources, GaSb and sulfur powders, are placed within two separate boron nitride crucibles, with distances of 15 and 9 cm away from the sample, respectively. It is worth pointing out that the sulfur powder is placed in the middle of the two zones. During the growth, the source and substrate are heated to 750 and 545 °C, accordingly. Hydrogen (99.9995% purity) with a flow rate of 200 sccm is used as the carrier gas to transport the thermally vaporized precursors to the downstream. Prior to heating, the pressure of the quartz tube is pumped to 3×10^{-3} Torr and then purged with H_2 for 0.5 h. After the growth, the source and substrate heater are stopped together and cooled to room temperature under the hydrogen flow.

Material Characterization. Surface morphologies of the grown NWs are examined with a scanning electron microscope (SEM, FEI Company, OR/Philips XL30, Philips Electronics, Amsterdam, The Netherlands) and a transmission electron microscope (TEM, Philips CM-20). Crystal structures are determined by collecting XRD patterns on a Philips powder diffractometer using Cu Kα radiation (λ = 1.5406 Å) and imaging with a high resolution TEM (HRTEM, JEOL 2100F, JEOL Co., Ltd., Tokyo, Japan). Elemental mappings are performed using an energy dispersive X-ray (EDS) detector attached to the JEOL 2100F to measure the chemical composition of the grown NWs. The chemical state of the as-prepared GaSb NWs is examined by X-ray photoelectron spectroscopy (XPS, ULVAC-PHI, Inc., model 5802, Kanagawa, Japan). For the TEM and elemental mappings, the NWs are first suspended in the ethanol solution by ultrasonication and drop-casted onto the grid for the corresponding characterization.

Nanowire FET Fabrication and Measurements. NWFETs are fabricated by drop-casting the NW suspension onto highly doped p-type Si substrates with a 50 nm thick thermally grown gate oxide. Photolithography is utilized to define the source and drain regions and 60 nm thick Ni film is thermally deposited as the contact electrodes followed by a lift-off process. The electrical performance of the fabricated back-gated FETs is then characterized with a standard electrical probe station and an Agilent 4155C semiconductor analyzer (Agilent Technologies, Santa Clara, CA).

Atomic Model. All atomic models are established by Materials Studio 5.0.

Conflict of Interest: The authors declare no competing financial interest.

Acknowledgment. We acknowledge the General Research Fund of the Research Grants Council of Hong Kong SAR, China, under Project Number CityU 101111, the National Natural Science Foundation of China (Grants 51202205), the State Key Laboratory of Multiphase Complex Systems (MPCS-2014-C-01), the Science Technology and Innovation Committee of Shenzhen Municipality (Grant JCYJ20140419115507588), and a grant from the Shenzhen Research Institute, City University of Hong Kong.

Supporting Information Available: The Supporting Information is available free of charge on the ACS Publications website at DOI: 10.1021/acsnano.5b04152.

Electron microscopy of the as-grown GaSb NWs; possible configurations of Sb dangling bonds (DBs) existed on the NW surfaces with different growth orientations; a typical atomic model for calculating the amount of Sb dangling bonds (DBs) and their density; Gauss−Lorentz fitted XPS spectra; electrical characterization of fabricated GaSb NWFETs and calculation details on field-effect hole mobility and hole concentration (PDF)

Note Added after ASAP Publication: This paper was published ASAP on August 24, 2015. Figure 3 was replaced and the revised version was reposted on August 26, 2015.

REFERENCES AND NOTES

1. Del Alamo, J. A. Nanometre-scale Electronics with III-V Compound Semiconductors. *Nature* **2011**, *479*, 317–323.
2. Han, N.; Wang, F.; Hou, J. J.; Yip, S. P.; Lin, H.; Xiu, F.; Fang, M.; Yang, Z.; Shi, X.; Dong, G.; Ho, J. C. Tunable Electronic Transport Properties of Metal-Cluster-Decorated III-V Nanowire Transistors. *Adv. Mater.* **2013**, *25*, 4445–4451.
3. Yang, Z.-X.; Han, N.; Wang, F.; Cheung, H.-Y.; Shi, X.; Yip, S.; Hung, T.; Lee, M. H.; Wong, C.-Y.; Ho, J. C. Carbon Doping of InSb Nanowires for High-Performance P-channel Field-Effect-Transistors. *Nanoscale* **2013**, *5*, 9671–9676.
4. Li, X.; Wei, X.; Xu, T.; Pan, D.; Zhao, J.; Chen, Q. Remarkable and Crystal-Structure-Dependent Piezoelectric and Piezoresistive Effects of InAs Nanowires. *Adv. Mater.* **2015**, *27*, 2852–2858.
5. Cheung, H.; Yip, S.; Han, N.; Dong, G.; Fang, M.; Yang, Z.-X.; Wang, F.; Lin, H.; Wong, C.-Y.; Ho, J. C. Modulating Electrical Properties of InAs Nanowires *via* Molecular Monolayers. *ACS Nano* **2015**, *9*, 7545–7552.
6. Al-Zahrani, H. Y.; Pal, J.; Migliorato, M. A.; Tse, G.; Yu, D. Piezoelectric Field Enhancement in III−V Core−Shell Nanowires. *Nano Energy* **2015**, *14*, 382–391.
7. Roddaro, S.; Ercolani, D.; Safeen, M. A.; Suomalainen, S.; Rossella, F.; Giazotto, F.; Sorba, L.; Beltram, F. Giant Thermovoltage in Single InAs Nanowire Field-Effect Transistors. *Nano Lett.* **2013**, *13*, 3638–3642.
8. Chang, W.; Albrecht, S.; Jespersen, T.; Kuemmeth, F.; Krogstrup, P.; Nygård, J.; Marcus, C. Hard Gap in Epitaxial Semiconductor-Superconductor Nanowires. *Nat. Nanotechnol.* **2015**, *10*, 232–236.
9. Huang, M. H.; Mao, S.; Feick, H.; Yan, H.; Wu, Y.; Kind, H.; Weber, E.; Russo, R.; Yang, P. Room-Temperature Ultraviolet Nanowire Nanolasers. *Science* **2001**, *292*, 1897–1899.
10. Ma, L.; Hu, W.; Zhang, Q.; Ren, P.; Zhuang, X.; Zhou, H.; Xu, J.; Li, H.; Shan, Z.; Wang, X. Room-Temperature Near-Infrared Photodetectors Based on Single Heterojunction Nanowires. *Nano Lett.* **2014**, *14*, 694–698.
11. Miao, J.; Hu, W.; Guo, N.; Lu, Z.; Zou, X.; Liao, L.; Shi, S.; Chen, P.; Fan, Z.; Ho, J. C.; et al. Single InAs Nanowire Room-Temperature Near-Infrared Photodetectors. *ACS Nano* **2014**, *8*, 3628–3635.
12. Loitsch, B.; Rudolph, D.; Morkötter, S.; Döblinger, M.; Grimaldi, G.; Hanschke, L.; Matich, S.; Parzinger, E.; Wurstbauer, U.; Abstreiter, G.; et al. Tunable Quantum Confinement in Ultrathin, Optically Active Semiconductor Nanowires *via* Reverse-Reaction Growth. *Adv. Mater.* **2015**, *27*, 2195–2202.
13. Wallentin, J.; Anttu, N.; Asoli, D.; Huffman, M.; Åberg, I.; Magnusson, M. H.; Siefer, G.; Fuss-Kailuweit, P.; Dimroth, F.; Witzigmann, B.; et al. InP Nanowire Array Solar Cells Achieving 13.8% Efficiency by Exceeding the Ray Optics Limit. *Science* **2013**, *339*, 1057–1060.
14. Nowzari, A.; Heurlin, M.; Jain, V.; Storm, K.; Hosseinnia, A.; Anttu, N.; Borgstrom, M. T.; Pettersson, H. k.; Samuelson, L. A Comparative Study of Absorption in Vertically and Laterally Oriented InP Core−Shell Nanowire Photovoltaic Devices. *Nano Lett.* **2015**, *15*, 1809–1814.
15. Mohseni, P. K.; Behnam, A.; Wood, J. D.; Zhao, X.; Yu, K. J.; Wang, N. C.; Rockett, A.; Rogers, J. A.; Lyding, J. W.; Pop, E.; et al. Monolithic III-V Nanowire Solar Vells on Graphene *via* Direct Van Der Waals Epitaxy. *Adv. Mater.* **2014**, *26*, 3755–3760.
16. Borg, B. M.; Dick, K. A.; Ganjipour, B.; Pistol, M.-E.; Wernersson, L.-E.; Thelander, C. InAs/GaSb Heterostructure Nanowires for Tunnel Field-Effect Transistors. *Nano Lett.* **2010**, *10*, 4080–4085.
17. Dey, A. W.; Svensson, J.; Borg, B. M.; Ek, M.; Wernersson, L.-E. Single InAs/GaSb Nanowire Low-Power CMOS Inverter. *Nano Lett.* **2012**, *12*, 5593–5597.
18. Ganjipour, B.; Dey, A. W.; Borg, B. M.; Ek, M.; Pistol, M.-E.; Dick, K. A.; Wernersson, L.-E.; Thelander, C. High Current Density Esaki Tunnel Diodes Based on GaSb-InAsSb Heterostructure Nanowires. *Nano Lett.* **2011**, *11*, 4222–4226.
19. Ganjipour, B.; Nilsson, H. A.; Borg, B. M.; Wernersson, L.-E.; Samuelson, L.; Xu, H.; Thelander, C. GaSb Nanowire Single-Hole Transistor. *Appl. Phys. Lett.* **2011**, *99*, 262104.
20. Nah, J.; Fang, H.; Wang, C.; Takei, K.; Lee, M. H.; Plis, E.; Krishna, S.; Javey, A. III−V Complementary Metal-Oxide-

Semiconductor Electronics on Silicon Substrates. *Nano Lett.* **2012**, *12*, 3592–3595.
21. Yang, Z.-X.; Han, N.; Fang, M.; Lin, H.; Cheung, H.-Y.; Yip, S.; Wang, E.-J.; Hung, T.; Wong, C.-Y.; Ho, J. C. Surfactant-Assisted Chemical Vapour Deposition of High-Performance Small-Diameter GaSb Nanowires. *Nat. Commun.* **2014**, *5*, 5249.
22. Yang, Z.-X.; Wang, F.; Han, N.; Lin, H.; Cheung, H.-Y.; Fang, M.; Yip, S.; Hung, T.; Wong, C.-Y.; Ho, J. C. Crystalline GaSb Nanowires Synthesized on Amorphous Substrates: from the Formation Mechanism to P-Channel Transistor Applications. *ACS Appl. Mater. Interfaces* **2013**, *5*, 10946–10952.
23. Burke, R. A.; Weng, X.; Kuo, M.-W.; Song, Y.-W.; Itsuno, A. M.; Mayer, T. S.; Durbin, S. M.; Reeves, R. J.; Redwing, J. M. Growth and Characterization of Unintentionally Doped GaSb Nanowires. *J. Electron. Mater.* **2010**, *39*, 355–364.
24. Jeppsson, M.; Dick, K. A.; Nilsson, H. A.; Sköld, N.; Wagner, J. B.; Caroff, P.; Wernersson, L.-E. Characterization of GaSb Nanowires Grown by MOVPE. *J. Cryst. Growth* **2008**, *310*, 5119–5122.
25. Xu, G.; Huang, S.; Wang, X.; Yu, B.; Zhang, H.; Yang, T.; Xu, H.; Dai, L. Synthesis, Properties, and Top-Gated Metal-Oxide-Semiconductor Field-Effect Transistors of P-Type GaSb Nanowires. *RSC Adv.* **2013**, *3*, 19834–19839.
26. Zi, Y.; Zhao, Y.; Candebat, D.; Appenzeller, J.; Yang, C. Synthesis of Antimony-Based Nanowires Using the Simple Vapor Deposition Method. *ChemPhysChem* **2012**, *13*, 2585–2588.
27. Ek, M.; Borg, B. M.; Johansson, J.; Dick, K. A. Diameter Limitation in Growth of III-Sb-Containing Nanowire Heterostructures. *ACS Nano* **2013**, *7*, 3668–3675.
28. Borg, B. M.; Wernersson, L.-E. Synthesis and Properties of Antimonide Nanowires. *Nanotechnology* **2013**, *24*, 202001.
29. Allen, J. E.; Perea, D. E.; Hemesath, E. R.; Lauhon, L. J. Nonuniform Nanowire Doping Profiles Revealed by Quantitative Scanning Photocurrent Microscopy. *Adv. Mater.* **2009**, *21*, 3067–3072.
30. Perea, D. E.; Hemesath, E. R.; Schwalbach, E. J.; Lensch-Falk, J. L.; Voorhees, P. W.; Lauhon, L. J. Direct Measurement of Dopant Ddistribution in an Individual Vapour-Liquid-Solid Nanowire. *Nat. Nanotechnol.* **2009**, *4*, 315–319.
31. Cai, Y.; Chan, S. K.; Sou, I. K.; Chan, Y. F.; Su, D. S.; Wang, N. The Size-Dependent Growth Direction of ZnSe Nanowires. *Adv. Mater.* **2006**, *18*, 109–114.
32. Schmidt, V.; Senz, S.; Gösele, U. Diameter-Dependent Growth Direction of Epitaxial Silicon Nanowires. *Nano Lett.* **2005**, *5*, 931–935.
33. Wu, Y.; Cui, Y.; Huynh, L.; Barrelet, C. J.; Bell, D. C.; Lieber, C. M. Controlled Growth and Structures of Molecular-Scale Silicon Nanowires. *Nano Lett.* **2004**, *4*, 433–436.
34. Han, N.; Wang, F.; Hou, J. J.; Yip, S.; Lin, H.; Fang, M.; Xiu, F.; Shi, X.; Hung, T.; Ho, J. C. Manipulated Growth of GaAs Nanowires: Controllable Crystal Quality and Growth Orientations *via* a Supersaturation-Controlled Engineering Process. *Cryst. Growth Des.* **2012**, *12*, 6243–6249.
35. Han, N.; Hou, J. J.; Wang, F.; Yip, S.; Yen, Y.-T.; Yang, Z.-X.; Dong, G.; Hung, T.; Chueh, Y.-L.; Ho, J. C. GaAs Nanowires: from Manipulation of Defect Formation to Controllable Electronic Transport Properties. *ACS Nano* **2013**, *7*, 9138–9146.
36. Ford, A. C.; Ho, J. C.; Chueh, Y.-L.; Tseng, Y.-C.; Fan, Z.; Guo, J.; Bokor, J.; Javey, A. Diameter-Dependent Electron Mobility of InAs Nanowires. *Nano Lett.* **2009**, *9*, 360–365.
37. Hou, J. J.; Wang, F.; Han, N.; Zhu, H.; Fok, K.; Lam, W.; Yip, S.; Hung, T.; Lee, J. E.-Y.; Ho, J. C. Diameter Dependence of Electron Mobility in InGaAs Nanowires. *Appl. Phys. Lett.* **2013**, *102*, 093112.
38. Motayed, A.; Vaudin, M.; Davydov, A. V.; Melngailis, J.; He, M.; Mohammad, S. Diameter Dependent Transport Properties of Gallium Nitride Nanowire Field Effect Transistors. *Appl. Phys. Lett.* **2007**, *90*, 043104.
39. Kranzer, D. Mobility of Holes of Zinc-Blende III-V and II-VI Compounds. *Phys. Status Solidi A* **1974**, *26*, 11–52.
40. Wiley, J. Mobility of Holes in III-V Vompounds. *Semiconduct. Semimimet.* **1975**, *10*, 91–174.
41. Cui, Y.; Lauhon, L. J.; Gudiksen, M. S.; Wang, J.; Lieber, C. M. Diameter-Controlled Synthesis of Single-Crystal Silicon Nanowires. *Appl. Phys. Lett.* **2001**, *78*, 2214–2216.
42. Ford, A. C.; Ho, J. C.; Fan, Z.; Ergen, O.; Altoe, V.; Aloni, S.; Razavi, H.; Javey, A. Synthesis, Contact Printing, and Device Characterization of Ni-Catalyzed, Crystalline InAs Nanowires. *Nano Res.* **2008**, *1*, 32–39.
43. Han, N.; Wang, F.; Hou, J. J.; Xiu, F.; Yip, S.; Hui, A. T.; Hung, T.; Ho, J. C. Controllable P−N Switching Behaviors of GaAs Nanowires *via* an Interface Effect. *ACS Nano* **2012**, *6*, 4428–4433.
44. Car, D.; Wang, J.; Verheijen, M. A.; Bakkers, E. P.; Plissard, S. R. Rationally Designed Single-Crystalline Nanowire Networks. *Adv. Mater.* **2014**, *26*, 4875–4879.
45. Rao, C.; Kulkarni, G.; Thomas, P. J.; Edwards, P. P. Size-Dependent Chemistry: Properties of Nanocrystals. *Chem.—Eur. J.* **2002**, *8*, 28–35.
46. Volokitin, Y.; Sinzig, J.; De Jongh, L.; Schmid, G.; Vargaftik, M.; Moiseevi, I. Quantum-Size Effects in the Thermodynamic Properties of Metallic Nanoparticles. *Nature* **1996**, *384*, 621–623.
47. Wang, F.; Yip, S.; Han, N.; Fok, K.; Lin, H.; Hou, J. J.; Dong, G.; Hung, T.; Chan, K.; Ho, J. C. Surface Roughness Induced Electron Mobility Degradation in InAs Nanowires. *Nanotechnology* **2013**, *24*, 375202.